Inorg. Chem. **2006**, *45*, 7372–7381

Reactivity and Structural and Physical Studies of Tetranuclear Iron(III) Clusters Containing the $[Fe_4(\mu_3\text{-}O)_2]^{8+}$ "Butterfly" Core: an Fe^{III}_4 Cluster with an $S = 1$ Ground State

Theocharis C. Stamatatos,[†] Athanassios K. Boudalis,[‡] Yiannis Sanakis,[‡] and Catherine P. Raptopoulou*[,‡]

Department of Chemistry, University of Patras, 26504 Patras, Greece, and Institute of Materials Science, NCSR "Demokritos", 15310 Aghia Paraskevi, Athens, Greece

Received March 22, 2006

The initial use of di-2-pyridyl ketone oxime [$(py)_2$CNOH] in iron(III) carboxylate chemistry has yielded the tetranuclear complex $[Fe_4O_2Cl_2(O_2CMe)_2\{(py)_2CNO\}_4]$ (**1**). Compound **1** can be synthesized either by the 1:2:1 molar ratio reaction between Fe^{III}, $MeCO_2^-$, and $(py)_2$CNOH (complex **1a**) or by the 1:3 molar ratio reaction between $[Fe_3O(O_2CMe)_6(H_2O)_3]Cl$ and $(py)_2$CNOH (complex **1b**). The presence of N_3^- in both reaction mixtures has afforded the tetranuclear complex $[Fe_4O_2(N_3)_2(O_2CMe)_2\{(py)_2CNO\}_4]$ (**2**), which can be alternatively synthesized by the reaction of **1** with N_3^-. Compound **1a** crystallizes in the tetragonal space group $I\bar{4}$ with (at 25 °C) $a = 35.06(2)$ Å, $b = 35.06(2)$ Å, $c = 13.255(6)$ Å, $V = 16293(2)$ Å^3, and $Z = 8$. Compound **1b** crystallizes in the monoclinic space group $P2_1/c$ with (at 25 °C) $a = 22.577(7)$ Å, $b = 17.078(6)$ Å, $c = 17.394(6)$ Å, $\beta = 93.50(1)°$, $V = 6694(4)$ Å^3, and $Z = 4$. Compound **2** crystallizes in the triclinic space group $P\bar{1}$ with (at 25 °C) $a = 13.658(9)$ Å, $b = 15.815(9)$ Å, $c = 17.29(1)$ Å, $\alpha = 97.08(3)°$, $\beta = 98.55(3)°$, $\gamma = 112.12(3)°$, $V = 3355(4)$ Å^3, and $Z = 2$. The structures of **1** and **2** contain the $[Fe_4(\mu_3\text{-}O)_2]^{8+}$ core comprising four Fe^{III} ions in a "butterfly" disposition and two μ_3-O^{2-} ions, each bridging three Fe^{III} ions forming the "wings" of the "butterfly". The Mössbauer spectra of **1b** and **2** consist of composite quadrupole-split doublets, with parameters typical for high-spin Fe^{III} in octahedral environments. Magnetic susceptibility measurements on **1a** revealed antiferromagnetic interactions between the $S = {}^5/_2$ ferric ions, with best-fit parameters being $J_{wb} = -40.2$ cm^{-1} and $J_{bb} = -59.4$ cm^{-1} ($H = -2\sum J_i J_j$) for wingtip–body and body–body interactions, respectively, yielding an $S = 1$ ground state. Both wingtip–body and body–body interactions are well determined.

Introduction

Technological applications nowadays are driven by the demand of miniaturization of devices, down to the molecular level. In order for this to happen, a breakthrough has to take place and new chemical species of nanometer size have to be synthesized to replace existing materials. Polynuclear metal complexes (clusters) have been proposed as potential materials for technological applications[1] because of their interesting properties (magnetic,[2] electronic,[3] optical,[4] catalytic,[5] etc.). Therefore, the biggest challenge for chemists today is the development of new nanometer-size molecular

* To whom correspondence should be addressed. E-mail: craptop@ims.demokritos.gr. Tel: +3210-6503365. Fax: +3210-6519430.
[†] University of Patras.
[‡] NCSR "Demokritos".

(1) (a) Leuenberger, M. N.; Loss, D. *Nature* **2001**, *410*, 789. (b) Cavallini, M.; Gomez-Segura, J.; Ruiz-Molina, D.; Massi, M.; Albonetti, C.; Rovira, C.; Veciana, J.; Biscarini, F. *Angew. Chem., Int. Ed.* **2005**, *44*, 888.

(2) For recent examples involving Mn and Fe complexes, see: (a) Tasiopoulos, A. J.; Vinslava, A.; Wernsdorfer, W.; Abboud, K. A.; Christou, G. *Angew. Chem., Int. Ed.* **2004**, *43*, 2117. (b) Soler, M.; Wernsdorfer, W.; Folting, K.; Pink, M.; Christou, G. *J. Am. Chem. Soc.* **2004**, *126*, 2156. (c) Aliaga-Alcalde, N.; Edwards, R. S.; Hill, S. O.; Wernsdorfer, W.; Folting, K.; Christou, G. *J. Am. Chem. Soc.* **2004**, *126*, 12503. (d) Wang, S.; Zuo, J.-L.; Zhou, H.-C.; Choi, H. J.; Ke, Y.; Long, J. R.; You, X.-Z. *Angew. Chem., Int. Ed.* **2004**, *43*, 5940. (e) Oshio, H.; Hoshino, N.; Ito, T.; Nakano, M. *J. Am. Chem. Soc.* **2004**, *126*, 8805.

(3) (a) Yu, G.; Yin, S.; Liu, Y.; Shuai, Z.; Zhu, D. *J. Am. Chem. Soc.* **2003**, *125*, 14816. (b) Bordiga, S.; Lamberti, C.; Ricchiardi, G.; Regli, L.; Bonino, F.; Damin, A.; Lillerud, K.-P.; Bjorgen, M.; Zecchina, A. *Chem. Commun.* **2004**, 2300. (c) Shi, J.-M.; Xu, W.; Liu, Q,-V.; Liu, F.-I.; Huang, Z.-I.; Lei, H.; Yu, W.-T.; Fang, Q. *Chem. Commun.* **2002**, 756. (d) Coronado, E.; Clemente-León, M.; Galán-Mascarós, J. R.; Giménez-Saiz, C.; Gómez-García, C. J.; Martínez-Ferrero, E. *J. Chem. Soc., Dalton Trans.* **2000**, 3955.

10.1021/ic0604821 CCC: $33.50
Published on Web 08/08/2006

Chart 1. Crystallographically Established Coordination Modes of the Anion $(py)_2CNO^-$ in Metal Complexes

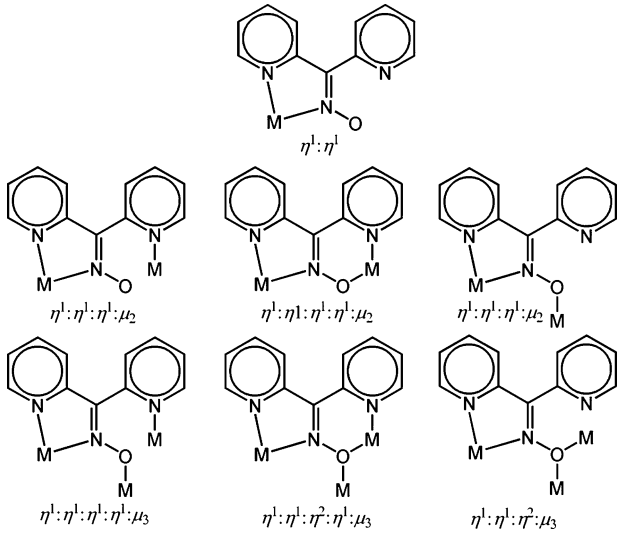

materials, such as metal clusters, with the desired properties. Unfortunately, the only effective way to fulfill this goal still remains the employment of the "trial and error" method.[6] Because serendipity still governs the synthesis of polynuclear metal clusters, the investigation of various reaction systems remains the best means to that end.

Our approach to the field is through the development of molecular magnetic materials based on 3d metal clusters. For this purpose, we have started a program concerning the investigation of reaction systems consisting of Fe^{III} and various polydentate ligands in the presence of carboxylates, and we have already reported our results concerning the use of salicylaldehyde oxime in iron(III) carboxylate chemistry.[7] In this work, we report our results concerning the initial use of di-2-pyridyl ketone oxime [$(py)_2CNOH$] (IUPAC name: di-pyridin-2-yl methanone oxime) in iron(III) carboxylate chemistry. The choice of $(py)_2CNOH$ was mainly based on three reasons: (1) the ability of its anion to coordinate to metal ions through either one, or both, N and O atoms of the oximato group, as well as either one, or both, pyridyl groups, acting as a chelating terminal or bridging ligand (Chart 1), (2) the interesting feature of activation of $(py)_2CNOH$ by 3d metal centers, which appears to be a fruitful area of synthetic inorganic chemistry,[8] and (3) the coordination chemistry of $(py)_2CNOH$ with Fe^{III} metal ions is still unexplored. Indeed, there are only a few examples of Zn,[9] Mn,[10] Ni,[11] Co,[12] Cu,[13] Au,[14] Ag,[13c] Re,[15] Os,[16] and Ru[16] complexes reported so far, but no Fe complexes have been reported. Most of these complexes belong to the family of the ring clusters with the $[M-N-O]_n$ repeating unit, also named metallacrowns.[17]

Herein we report the syntheses and structural and spectroscopic (IR and ^{57}Fe Mössbauer) studies of the first iron(III) carboxylate complexes of di-2-pyridyl ketone oxime, the tetranuclear compounds $[Fe_4O_2X_2(O_2CMe)_2\{(py)_2CNO\}_4]$ [$X^- = Cl^-$ (**1**) or N_3^- (**2**)]. We also report the magnetic study of **1**.

Experimental Section

Materials and Physical Measurements. All manipulations were performed under aerobic conditions using materials as received (Aldrich Co). All chemicals and solvents were reagent grade. $[Fe_3O(O_2CMe)_6(H_2O)_3]Cl$ was synthesized as previously described.[18] Elemental analyses for C, H, and N were performed using a Perkin-Elmer 2400/II automatic analyzer. IR spectra were recorded as KBr pellets in the range 4000−400 cm^{-1} on a Bruker Equinox 55/S Fourier transform (FT)-IR spectrometer. Mössbauer spectra were taken with a constant-acceleration spectrometer using a ^{57}Co

(4) (a) Niu, Y.; Song, Y.; Hou, H.; Zhu, Y. *Inorg. Chem.* **2005**, *44*, 2553. (b) Susumu, K.; Duncan, T. V.; Therien, M. J. *J. Am. Chem. Soc.* **2005**, *127*, 5186. (c) Meng, X.; Song, Y.; Hou, H.; Fan, Y.; Li, G.; Zhu, Y. *Inorg. Chem.* **2003**, *42*, 1306. (d) Tian, L.; Zhang, W.; Yang, B.; Lu, P.; Zhang, M.; Lu, D.; Ma, Y.; Shen, J. *J. Phys. Chem. B* **2005**, *109*, 6944. (e) Hou, H.; Wei, Y.; Song, Y.; Mi, L.; Tang, M.; Li, L.; Fan, Y. *Angew. Chem., Int. Ed.* **2005**, *44*, 6067.

(5) Although literature is abundant for various first-row metal complexes, for recent representative examples involving Fe complexes, see: (a) Legros, L.; Bolm, C. *Chem.—Eur. J.* **2005**, *11*, 1086. (b) Avenier, F.; Dubois, L.; Dubourdeaux, P.; Latour, J.-M. *Chem. Commun.* **2005**, 480. (c) Bénisvy, L.; Chottard, J.-C.; Marrot, J.; Li, Y. *Eur. J. Inorg. Chem.* **2005**, 999.

(6) Winpenny, R. E. P. *J. Chem. Soc., Dalton Trans.* **2002**, 1.

(7) (a) Raptopoulou, C. P.; Sanakis, Y.; Boudalis, A. K.; Psycharis, V. *Polyhedron* **2005**, *24*, 711. (b) Raptopoulou, C. P.; Boudalis, A. K.; Sanakis, Y.; Psycharis, V.; Clemente-Juan, J. M.; Fardis, M.; Diamantopoulos, G.; Papavassiliou, G. *Inorg. Chem.* **2006**, *45*, 2317.

(8) (a) For a comprehensive review on the coordination chemistry of pyridyl oximes, including di-2-pyridyl ketone oxime, see: Milios, C. J.; Stamatatos, Th. C.; Perlepes, S. P. *Polyhedron* **2006**, *25*, 134. (b) Kumagai, H.; Endo, M.; Kondo, M.; Kawata, S.; Kitagawa, S. *Coord. Chem. Rev.* **2003**, *237*, 197.

(9) (a) Stemmler, A. J.; Kampf, J. W.; Pecoraro, V. L. *Inorg. Chem.* **1995**, *34*, 2271. (b) Alexiou, M.; Dendrinou-Samara, C.; Raptopoulou, C. P.; Terzis, A.; Kessissoglou, D. P. *Inorg. Chem.* **2002**, *41*, 4732. (c) Alexiou, M.; Katsoulakou, E.; Dendrinou-Samara, C.; Raptopoulou, C. P.; Psycharis, V.; Manessi-Zoupa, E.; Perlepes, S. P.; Kessissoglou, D. P. *Eur. J. Inorg. Chem.* **2005**, 1964.

(10) (a) Afrati, T.; Dendrinou-Samara, C.; Raptopoulou, C. P.; Terzis, A.; Tangoulis, V.; Kessissoglou, D. P. *Angew. Chem., Int. Ed.* **2002**, *41*, 2148. (b) Dendrinou-Samara, C.; Zaleski, C. M.; Evagorou, A.; Kampf, J. W.; Pecoraro, V. L.; Kessissoglou, D. P. *Chem. Commun.* **2003**, 2668. (c) Alexiou, M.; Zaleski, C. M.; Dendrinou-Samara, C.; Kampf, J.; Kessissoglou, D. P.; Pecoraro, V. L. *Z. Anorg. Allg. Chem.* **2003**, *629*, 2348. (d) Milios, C. J.; Raptopoulou, C. P.; Terzis, A.; Vicente, R.; Escuer, A.; Perlepes, S. P. *Inorg. Chem. Commun.* **2003**, *6*, 1056. (e) Alexiou, M.; Dendrinou-Samara, C.; Karagianni, A.; Biswas, S.; Zaleski, C. M.; Kampf, J.; Yoder, D.; Penner-Hahn, J. E.; Pecoraro, V. L.; Kessissoglou, D. P. *Inorg. Chem.* **2003**, *42*, 2185. (f) Milios, C. J.; Kyritsis, P.; Raptopoulou, C. P.; Terzis, A.; Vicente, R.; Escuer, A.; Perlepes, S. P. *J. Chem. Soc., Dalton Trans.* **2005**, 501.

(11) (a) Psomas, G.; Dendrinou-Samara, C.; Alexiou, M.; Tsohos, A.; Raptopoulou, C. P.; Terzis, A.; Kessissoglou, D. P. *Inorg. Chem.* **1998**, *37*, 6556. (b) Alexiou, M.; Tsivikas, I.; Dendrinou-Samara, C.; Pantazaki, A. A.; Trikalitis, P.; Lalioti, N.; Kyriakidis, D. A.; Kessissoglou, D. P. *J. Inorg. Biochem.* **2003**, *93*, 256. (c) Alexiou, M.; Dendrinou-Samara, C.; Raptopoulou, C. P.; Terzis, A.; Tangoulis, V.; Kessissoglou, D. P. *Eur. J. Inorg. Chem.* **2004**, 3822.

(12) Stamatatos, Th. C.; Dionyssopoulou, S.; Efthymiou, G.; Kyritsis, P.; Raptopoulou, C. P.; Terzis, A.; Vicente, R.; Escuer, A.; Perlepes, S. P. *Inorg. Chem.* **2005**, *44*, 3374.

(13) (a) Schlemper, E. O.; Stunkel, J.; Patterson, C. *Acta Crystallogr.* **1990**, *C46*, 1226. (b) Goher, M. A. S.; Mautner, F. A. *Polyhedron* **1999**, *18*, 3425. (c) Sommerer, S. O.; Westcott, B. L.; Jircitano, A. J.; Abboud, K. A. *Inorg. Chim. Acta* **1995**, *238*, 149.

(14) Sommerer, S. O.; MacBeth, C. E.; Jircitano, A. J.; Abboud, K. A. *Acta Crystallogr.* **1997**, *C53*, 1551.

(15) Bakir, M. *Acta Crystallogr.* **2001**, *C57*, 1154.

(16) Cabeza, J. A.; del Rio, I.; Riera, V.; Suarez, M.; Alvarez-Rua, C.; Garcia-Granda, S.; Chuang, S. H.; Hwu, J. R. *Eur. J. Inorg. Chem.* **2003**, 4159.

(17) Pecoraro, V. L.; Stemmler, A. J.; Gibney, B. R.; Bodwin, J. J.; Wang, H.; Kampf, J. W.; Barwinski, A. *Prog. Inorg. Chem.* **1997**, *45*, 83.

(18) Anson, C. E.; Bourke, J. P.; Cannon, R. D.; Jayasooriya, U. A.; Molinier, M.; Powell, A. K. *Inorg. Chem.* **1997**, *36*, 1265.

(Rh matrix) source at room temperature and a variable-temperature Oxford cryostat. Variable-temperature magnetic susceptibility measurements were carried out on polycrystalline samples of **1a** in the 2.0−300 K temperature range using a Quantum Design MPMS SQUID susceptometer under a magnetic field of 1.0 T. A magnetization isotherm was collected at 2 K between 0 and 5.4 T. Data were corrected with standard procedures for the contribution of the sample holder and diamagnetism of the sample. The calculation of the magnetic susceptibility was accomplished by analytical calculation of the energy levels associated with the spin Hamiltonian. Minimization was carried out with an adapted version of *MINUIT*.[19] The error factor *R* is defined as

$$R = \sum \frac{(x_{exp} - x_{calc})^2}{N x_{exp}^2}$$

where *N* is the number of experimental points. Simulations of the magnetization *M* versus applied field *H* were carried out with the *MAGPACK* program package, using parameters derived from fits of the magnetic susceptibility.[20]

Caution! *Although no such behavior was observed during the present work, azides are potentially explosive and should be handled with care.*

$[Fe_4O_2Cl_2(O_2CMe)_2\{(py)_2CNO\}_4]\cdot 2CH_2Cl_2\cdot H_2O$ ($1a\cdot 2CH_2Cl_2\cdot H_2O$). To a stirred orange solution of $FeCl_3\cdot 6H_2O$ (0.081 g, 0.30 mmol) in MeCN (20 mL) was added solid $(py)_2CNOH$ (0.060 g, 0.30 mmol). The resulting deep-red solution was stirred for 30 min, during which time solid $NaO_2CMe\cdot 3H_2O$ (0.082 g, 0.60 mmol) was added in small portions without any noticeable color change. The solvent was evaporated to dryness under reduced pressure, and most of the residue redissolved in CH_2Cl_2 (25 mL) to give a deep-red solution. This was layered with a mixture of Et_2O and *n*-hexane [50 mL; 1:1 (v/v)]. After several days, dark-red needles appeared, which were collected by filtration, washed with Et_2O (2 × 5 mL), and dried in vacuo over silica gel. The resulting powder was analyzed as solvent-free. Yield (based on Fe^{III}): 0.056 g (60%). Anal. Calcd for $C_{48}H_{38}Fe_4N_{12}O_{10}Cl_2$: C, 46.6; H, 3.1; N, 13.6; Found: C, 46.0; H, 3.2; N, 13.3. Main IR data (KBr pellet): $\tilde{\nu}$ 3404 (vs), 1595 (m), 1536 (s), 1466 (m), 1435 (vs), 1350 (w), 1264 (w), 1213 (w), 1157 (w), 1094 (vs), 1019 (m), 985 (w), 791 (w), 752 (w), 706 (m), 651 (m), 590 (m), 493 (w), 422 (w), 401 (w) cm^{-1}.

$[Fe_4O_2Cl_2(O_2CMe)_2\{(py)_2CNO\}_4]\cdot 4.5MeNO_2$ ($1b\cdot 4.5MeNO_2$). To a stirred orange suspension of $[Fe_3O(O_2CMe)_6(H_2O)_3]Cl$ (0.063 g, 0.10 mmol) in CH_2Cl_2 (25 mL) was added solid $(py)_2CNOH$ (0.060 g, 0.30 mmol). The resulting deep-red solution was stirred for 1 h and layered with a mixture of Et_2O and *n*-hexane [50 mL; 1:1 (v/v)]. After 3 days, dark-red needles appeared, which were collected by filtration, washed with Et_2O (2 × 5 mL), and dried in air. The needles proved to be unsuitable for single-crystal X-ray diffraction studies, so they were dissolved in $MeNO_2$ (10 mL), and the resulting red solution was left undisturbed for slow evaporation at room temperature. After 2 weeks, deep-red X-ray-quality rectangular crystals appeared, which were collected by filtration, washed with Et_2O (2 × 5 mL), and dried in vacuo over silica gel. The IR spectrum of this material was almost identical with that of compound **1a**. Yield (based on Fe^{III}): 0.040 g (43%). Anal. Calcd for $C_{52.5}H_{51.5}Fe_4N_{16.5}O_{19}Cl_2$: C, 41.7; H, 3.4; N, 15.3. Found: C, 41.5; H, 3.2; N, 15.4.

$[Fe_4O_2(N_3)_2(O_2CMe)_2\{(py)_2CNO\}_4]\cdot 2CH_2Cl_2\cdot 2.5H_2O$ ($2\cdot 2CH_2Cl_2\cdot 2.5H_2O$). Method A. To a stirred deep-red suspension of $[Fe_4O_2Cl_2(O_2CMe)_2\{(py)_2CNO\}_4]$ (0.124 g, 0.10 mmol) in CH_2Cl_2 (25 mL) was added solid NaN_3 (0.013 g, 0.20 mmol). The resulting deep-red slurry was stirred for a further 2 h, during which time all of the amount of NaN_3 was completely dissolved. The solution was filtered (to remove the precipitated NaCl) and layered with *n*-hexane (50 mL). After several days, dark-red rectangular crystals appeared, which were collected by filtration, washed with Et_2O (2 × 5 mL), and dried in vacuo over silica gel. The resulting powder was analyzed as solvent-free. Yield (based on Fe^{III}): 0.059 g (47%). Anal. Calcd for $C_{48}H_{38}Fe_4N_{18}O_{10}$: C, 46.1; H, 3.1; N, 20.1. Found: C, 45.1; H, 2.8; N, 19.9. Main IR data (KBr pellet): $\tilde{\nu}$ 3433 (m), 2063 (vs), 1595 (m), 1537 (s), 1463 (m), 1437 (s), 1346 (w), 1266 (w), 1214 (w), 1157 (w), 1116 (m), 1099 (s), 1019 (w), 995 (w), 977 (w), 786 (w), 745 (w), 706 (m), 646 (m), 588 (m), 520 (w), 489 (w), 420 (w), 403 (w) cm^{-1}.

Method B. To a stirred orange solution of $FeCl_3\cdot 6H_2O$ (0.081 g, 0.30 mmol) in MeCN (20 mL) was added solid $(py)_2CNOH$ (0.060 g, 0.30 mmol). The resulting deep-red solution was stirred for 30 min, during which time solid $NaO_2CMe\cdot 3H_2O$ (0.082 g, 0.60 mmol) and NaN_3 (0.039 g, 0.60 mmol) were added in small portions without any noticeable color change. The solvent was evaporated to dryness under reduced pressure, and a quantity of the residue redissolved in CH_2Cl_2 (25 mL) to give a deep-red solution. This was filtered and layered with a mixture of Et_2O and *n*-hexane [50 mL; 1:1 (v/v)]. After several days, dark-red rectangular crystals appeared, which were collected by filtration, washed with Et_2O (2 × 5 mL), and dried in air. The dried solid analyzed satisfactorily as **2**. The identity of the product was further confirmed by IR spectroscopic comparison with the authentic sample prepared according to method A. Yield (based on Fe^{III}): 0.055 g (60%).

Method C. To a stirred orange suspension of $[Fe_3O(O_2CMe)_6(H_2O)_3]Cl$ (0.063 g, 0.10 mmol) in MeCN (20 mL) was added solid $(py)_2CNOH$ (0.040 g, 0.20 mmol). The resulting deep-red solution was stirred for 10 min, and then solid NaN_3 (0.020 g, 0.30 mmol) was added without any noticeable color change. The resultant new solution was stirred for a further 1 h, filtered, and left undisturbed for slow evaporation at room temperature. After 6 days, dark-red rectangular crystals appeared, which were collected by filtration, washed with Et_2O (2 × 5 mL), and dried in air. The dried solid analyzed satisfactorily as **2**. The identity of the product was further confirmed by IR spectroscopic comparison with the authentic sample prepared according to method A. Yield (based on Fe^{III}): 0.071 g (75%).

X-ray Crystallographic Studies: Diffraction measurements were made on a Crystal Logic dual goniometer diffractometer using graphite-monochromated Mo radiation. Important crystal data and parameters for data collection are reported in Table 1. Unit cell dimensions were determined and refined by using the angular settings of 25 automatically centered reflections in the range $11° < 2\theta < 23°$. Three standard reflections, monitored every 97 reflections, showed less than 3% intensity fluctuation and no decay. Lorentz and polarization corrections were applied using Crystal Logic software. The structures were solved by direct methods using *SHELXS-86*[21] and refined by full-matrix least-squares techniques on F^2 with *SHELXL-97*.[22] In all three structures, the crystals showed

(19) James, F.; Roos, M. *MINUIT* Program, a System for Function Minimization and Analysis of the Parameters Errors and Correlations. *Comput. Phys. Commun*. **1975**, *10*, 345.

(20) (a) Borrás-Almenar, J. J.; Clemente-Juan, J. M.; Coronado, E.; Tsukerblat, B. S. *Inorg. Chem.* **1999**, *38*, 6081. (b) Borrás-Almenar, J. J.; Clemente-Juan, J. M.; Coronado, E.; Tsukerblat, B. S. *J. Comput. Chem.* **2001**, *22*, 985.

(21) Sheldrick, G. M. *SHELXS-86: Structure Solving Program*; University of Göttingen: Göttingen, Germany, 1986.

Table 1. Crystallographic Data for **1a**·$2CH_2Cl_2$·H_2O, **1b**·$4.5MeNO_2$, and **2**·$2CH_2Cl_2$·$2.5H_2O$

	1a·$2CH_2Cl_2$·H_2O	**1b**·$4.5MeNO_2$	**2**·$2CH_2Cl_2$·$2.5H_2O$
formula	$C_{50}H_{44}Cl_6Fe_4N_{12}O_{11}$	$C_{52.5}H_{51.5}Cl_2Fe_4N_{16.5}O_{19}$	$C_{50}H_{47}Cl_4Fe_4N_{18}O_{12.5}$
fw	1425.07	1511.90	1465.26
space group	$I\bar{4}$	$P2_1/c$	$P\bar{1}$
T, °C	25	25	25
λ, Å	Mo Kα (0.710 73 Å)	Mo Kα (0.710 73 Å)	Mo Kα (0.710 73 Å)
a, Å	35.06(2)	22.577(7)	13.658(9)
b, Å	35.06(2)	17.078(6)	15.815(9)
c, Å	13.255(6)	17.394(6)	17.29(1)
α, deg			97.08(3)
β, deg		93.50(1)	98.55(3)
γ, deg			112.12(3)
V, Å^3	16293(2)	6694(4)	3355(4)
Z	8	4	2
$\rho_{calcd}/\rho_{measd}$, g cm^{-3}	1.161/1.14	1.500/1.48	1.450/1.42
μ(Mo Ka), mm^{-1}	0.944	1.009	1.075
R1[a]	0.0849[b]	0.0752[c]	0.0793[d]
wR2[a]	0.2238[b]	0.1972[c]	0.2147[d]

[a] $w = 1/[\sigma^2(F_o^2) + (aP)^2 + bP]$ and $P = \max(F_o^2,0) + 2F_c^2/3$; $R1 = \sum(|F_o| - |F_c|)/\sum(|F_o|)$ and $wR2 = \{\sum[w(F_o^2 - F_c^2)^2]/\sum[w(F_o^2)^2]\}^{1/2}$. [b] For 4666 reflections with $I > 2\sigma(I)$. [c] For 4780 reflections with $I > 2\sigma(I)$. [d] For 6924 reflections with $I > 2\sigma(I)$.

poor diffraction ability (despite their sufficient size), and in each case, the data collection was stopped when the observed data were almost half of the collected ones. Nevertheless, the quality of the collected data was adequate to establish the structure of each of the complexes. For compound **1a**·$2CH_2Cl_2$·H_2O, H atoms were introduced at calculated positions as riding on bonded atoms. All non-H atoms were refined anisotropically, except two noncoordinated pyridyl rings (defined by N3 and N13, which were refined isotropically). Three crystallographically independent CH_2Cl_2 molecules were found, two of which were refined with occupation factors fixed at 10.50. Only the Cl atoms were refined anisotropically. Two crystallographically independent water molecules were found, which were refined isotropically with occupation factors fixed at 10.50. For compound **1b**·$4.5MeNO_2$, H atoms were introduced at calculated positions as riding on bonded atoms. All non-H atoms were refined anisotropically except of the nitromethane solvent molecules, which were refined isotropically. Five crystallographically independent $MeNO_2$ molecules were found, one of which was refined with occupation factors fixed at 10.50. For compound **2**·$2CH_2Cl_2$·$2.5H_2O$, H atoms were introduced at calculated positions as riding on bonded atoms. All non-H atoms were refined anisotropically, except the water solvents, which were refined isotropically with fixed occupation factors. Full details can be found in the CIF files deposited as Supporting Information.

Results and Discussion

Synthesis. Complex **1** can be obtained either by the 1:2:1 molar ratio reaction mixture $Fe^{III}/MeCO_2^-/(py)_2CNOH$ in MeCN (**1a**) or by the 1:3 molar ratio reaction between the "basic iron(III) acetate" complex, $[Fe_3O(O_2CMe)_6(H_2O)_3]Cl$, and di-2-pyridyl ketone oxime in CH_2Cl_2 (**1b**). The large excess of $NaO_2CMe·3H_2O$ used [$Fe^{III}/(py)_2CNOH/NaO_2CMe·3H_2O$ = 1:1:2 or 4:4:8] is beneficial to the preparation of **1a**. The excess of $MeCO_2^-$ helps the deprotonation of the neutral ligand $(py)_2CNOH$, and the so-formed weak acid ($MeCO_2H$) does not decompose the oxide-bridged cluster. The balanced chemical equation may be written in the form of **1a**. Of course, other species may be present in the reaction mixture, and the equations given below are not representative of all of the aggregates formed in solution.

$$4FeCl_3·6H_2O + 4(py)_2CNOH + 8NaO_2CMe·3H_2O \xrightarrow{MeCN} \underset{\mathbf{1a}}{[Fe_4O_2Cl_2(O_2CMe)_2\{(py)_2CNO\}_4]} + 8NaCl + 2HCl + 6MeCO_2H + 46H_2O \quad (1)$$

In this case, it is assumed that H_2O from the solvents and/or the starting materials is the source of the O^{2-} ions.

The balanced chemical equation for the synthesis of **1b** may be written in the form of eq 2.

$$6[Fe_3O(O_2CMe)_6(H_2O)_3]Cl + 12(py)_2CNOH \xrightarrow{CH_2Cl_2} 3\underset{\mathbf{1b}}{[Fe_4O_2Cl_2(O_2CMe)_2\{(py)_2CNO\}_4]} + 2"[Fe_3O(O_2CMe)_6(H_2O)_2(OH)]" + 18MeCO_2H + 10H_2O \quad (2)$$

Under the reaction conditions used, the propensity of the second pyridyl N atom of $(py)_2CNO^-$ toward coordination has not been realized, whereas, under the same conditions, the deprotonated oximate O atom is coordinated. The 1:1 $Fe^{III}/(py)_2CNOH$ molar ratio reaction is reflected in the stoichiometry of the final product. An excess of the metal ion in the reaction mixture may favor the synthesis of even higher nuclearity metal clusters, a possibility that is currently under investigation in our laboratory.

The presence of azides in the above reaction mixtures has not affected the identity of the final product, confirming that the $[Fe_4(\mu_3\text{-}O)_2]^{8+}$ core is stable enough not to be easily disrupted. As a result, the azides in **2** have been terminally coordinated to the Fe^{III} ions replacing the terminal Cl^- atoms in **1**. The synthesis of the tetranuclear compound **2** can be accomplished either by the reaction of **1** with NaN_3 (eq 3a) or by the addition of NaN_3 in the reaction mixtures that afforded complex **1** (eqs 3b and 3c, respectively). The

$$\underset{\mathbf{1}}{[Fe_4O_2Cl_2(O_2CMe)_2\{(py)_2CNO\}_4]} + 2NaN_3 \xrightarrow{CH_2Cl_2} \underset{\mathbf{2}}{[Fe_4O_2(N_3)_2(O_2CMe)_2\{(py)_2CNO\}_4]} + 2NaCl \quad (3a)$$

(22) Sheldrick, G. M. *SHELXL-97: Crystal Structure Refinement*; University of Göttingen: Göttingen, Germany, 1997.

$$4FeCl_3\cdot 6H_2O + 4(py)_2CNOH + 8NaO_2CMe\cdot 3H_2O + 2NaN_3 \xrightarrow{MeCN} \underset{\mathbf{2}}{[Fe_4O_2(N_3)_2(O_2CMe)_2\{(py)_2CNO\}_4]} + 10NaCl + 2HCl + 6MeCO_2H + 46H_2O \quad (3b)$$

$$6[Fe_3O(O_2CMe)_6(H_2O)_3]Cl + 12(py)_2CNOH + 6NaN_3 \xrightarrow{MeCN} 3\underset{\mathbf{2}}{[Fe_4O_2(N_3)_2(O_2CMe)_2\{(py)_2CNO\}_4]} + 2"[Fe_3O(O_2CMe)_6(H_2O)_2(OH)]" + 6NaCl + 18MeCO_2H + 10H_2O \quad (3c)$$

reactions leading to the synthesis of complexes **1** and **2** are summarized in Scheme 1.

Our previous experience concerning the use of salicylaldehyde oxime in iron(III) carboxylate chemistry showed that the oximato O atom can act either as terminal or as bridging to afford tri- or hexanuclear complexes, respectively.[7] On the other hand, the oximato O atom of the di-2-pyridyl ketone oxime in **1** and **2** is terminally coordinated, probably because of the steric effects exerted by the second pyridyl group bound to the cyanide C atom, with respect to the H atom in the case of salicylaldehyde oxime.

Description of the Structures. Compounds **1a** and **1b** are essentially the same and contain the tetranuclear species $[Fe_4O_2Cl_2(O_2CMe)_2\{(py)_2CNO\}_4]$ along with different solvate molecules as a result of the different synthetic routes and crystallization methods employed. The molecular structure of **1b** is depicted in Figure 1, and selected bond distances and angles are listed in Table 2 (selected bond distances and angles for complex **1a** are given in the Supporting Information Table S1). The tetranuclear molecules contain the $[Fe_4(\mu_3\text{-}O)_2]^{8+}$ core comprising four Fe^{III} ions in a "butterfly" disposition and two μ_3-O^{2-} ions, each bridging three Fe^{III} ions, forming the "wings" of the "butterfly". Atoms Fe2 and Fe3 occupy the "hinge" or "body" sites, and Fe1 and Fe4 occupy the "wingtip" positions. The topology of the central $[Fe_4(\mu_3\text{-}O)_2]^{8+}$ core can be also described as two edge-sharing $[Fe_3(\mu_3\text{-}O)]^{7+}$ triangular subunits. The dihedral angles between the least-squares plane defined by Fe1/Fe2/Fe3 and Fe2/Fe3/Fe4 are 179.5 and 175.0° for **1a** and **1b**, respectively; thus, the four Fe^{III} ions are essentially coplanar. As a result, the two μ_3-O^{2-} ions are forced to leave their respective $[Fe_3(\mu_3\text{-}O)]$ triangle and are displaced above and below the $[Fe_4]$ least-squares plane (ca. 0.5 Å). This is also reflected in the sums of the Fe−O−Fe angles around the μ_3-O^{2-} ions, which severely deviate from 360° (ca. 338°) and are close to the ideal value of 328.4° expected for pure sp^3 hybridization. A literature survey of tetranuclear complexes presenting the $[Fe_4(\mu_3\text{-}O)_2]^{8+}$ core showed a number of different configurations regarding the position of the "wing" metal ions and the displacement of the μ_3-O^{2-} ions with respect to their respective $[Fe_3]$ planes (Chart 2 and Table 4). However, in all cases the sum of the Fe−O−Fe angles around the μ_3-O^{2-} ion falls in the range 350−359°. Only in the case of $K_2[Fe_4(OH)_2(PO_4)_4(H_2O)_2]$[23] is the sum of the Fe−O−Fe angles around the μ_3-OH group 339.8°. In the cases of **1a** and **1b**, the two μ_3-O^{2-} ions show a more pyramidal character than that in analogous complexes. Each μ_3-O^{2-} ion presents two short (∼1.9 Å) and one longer (∼2.0 Å) Fe−O distance in both **1a** and **1b**, unlike the case of the more symmetrical $[Fe_3(\mu_3\text{-}O)]$ triangular units found in various "basic iron(III) carboxylates",[24] where the μ_3-O^{2-} ion is symmetrically coordinated to the Fe^{III} ions at ∼1.9 Å. The two short Fe−O bond distances exert a trans influence on the Fe−N bond (Fe−N ∼ 2.2 Å).

The two "body" Fe^{III} ions (Fe2 and Fe3) are bridged by two μ_3-oxides, while a single μ_3-oxide ion participates in the coordination sphere of the "wingtip" Fe^{III} ions. As a result, the central Fe2···Fe3 separation is much shorter (2.916 and 2.890 Å in **1a** and **1b**, respectively) than the body-to-wing separations, which fall in the range 3.257−3.385 Å in **1a** and 3.254−3.298 Å in **1b**. The wing-to-wing separation is the largest one as expected (5.965 and 5.968 Å in **1a** and **1b**, respectively).

The four di-2-pyridyl ketone oxime ligands are anionic, presenting the η^1:η^1:η^1:μ_2 coordination mode (Chart 1)

Scheme 1. Reaction Scheme for the Synthesis of Compounds **1** and **2** (L = Terminal Solvate Molecules; ∩ = Bidentate Bridging Acetate or $(py)_2CNO^-$ Ligands)

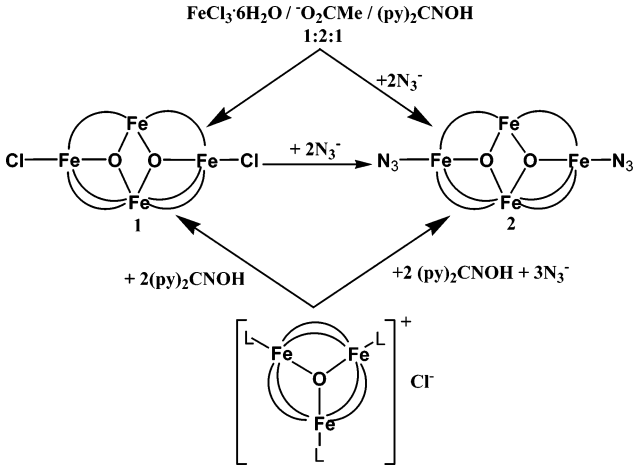

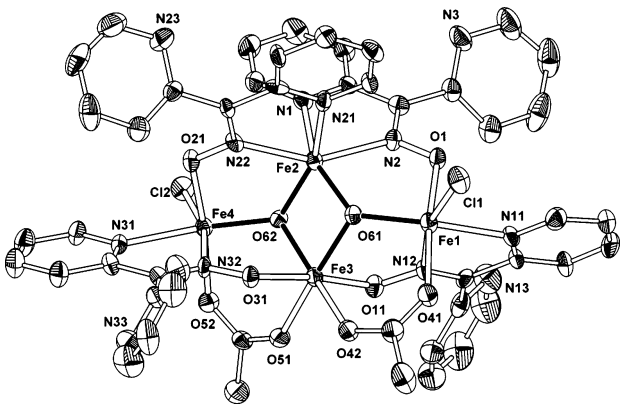

Figure 1. Partially labeled ORTEP plot of **1b** with ellipsoids drawn at the 30% probability level. H atoms have been omitted for clarity. Black bonds describe the $[Fe_4(\mu_3\text{-}O)_2]^{8+}$ core.

(23) Moore, P. B. *Am. Mineral.* **1972**, *57*, 397.

(24) Among many others, see, for example: (a) Gorun, S. M.; Papaefthymiou, G. C.; Frankel, R. B.; Lippard, S. J. *J. Am. Chem. Soc.* **1987**, *109*, 3337. (b) Bond, A. M.; Clark, R. J. H.; Humphrey, D. G.; Panayiotopoulos, P.; Skelton, B. W.; White, A. H. *J. Chem. Soc., Dalton Trans.* **1998**, 1845. (c) Degang, F.; Guoxiong, W.; Wenxia, T. *Polyhedron* **1993**, *20*, 2459.

Table 2. Selected Bond Distances (Å) and Angles (deg) in **1b**·4.5$MeNO_2$

		Distances			
Fe1−O61	1.855(6)	Fe2−O62	1.906(6)	Fe3−O61	1.978(6)
Fe1−O1	2.005(7)	Fe2−O61	1.918(6)	Fe3−O62	1.993(6)
Fe1−O41	2.031(7)	Fe2−N22	2.138(9)	Fe3−O11	2.013(7)
Fe1−N12	2.156(9)	Fe2−N2	2.160(8)	Fe3−O51	2.017(7)
Fe1−N11	2.197(10)	Fe2−N21	2.178(9)	Fe3−O42	2.030(7)
Fe1−Cl1	2.286(3)	Fe2−N1	2.198(8)	Fe3−O31	2.030(7)
Fe4−O62	1.875(6)	Fe4−O52	2.036(7)	Fe4−N31	2.202(8)
Fe4−O21	2.024(7)	Fe4−N32	2.161(8)	Fe4−Cl2	2.304(3)
Fe1···Fe2	3.398(2)	Fe1···Fe3	3.254(2)	Fe1···Fe4	5.968(2)
Fe2···Fe3	2.890(10)	Fe2···Fe4	3.371(2)	Fe3···Fe4	3.260(2)
		Angles			
O61−Fe1−O1	89.7(3)	O62−Fe2−O61	86.1(3)	O62−Fe3−O61	82.2(3)
O61−Fe1−O41	95.8(3)	O62−Fe2−N22	83.3(3)	O61−Fe3−O11	89.8(3)
O1−Fe1−O41	169.9(3)	O61−Fe2−N22	116.9(3)	O62−Fe3−O11	93.1(3)
O61−Fe1−N12	87.5(3)	O62−Fe2−N2	115.6(3)	O61−Fe3−O51	172.4(3)
O1−Fe1−N12	86.6(3)	O61−Fe2−N2	83.6(3)	O51−Fe3−O62	94.5(3)
O41−Fe1−N12	85.2(3)	N22−Fe2−N2	154.0(3)	O51−Fe3−O11	83.6(3)
O61−Fe1−N11	156.9(3)	O62−Fe2−N21	153.8(3)	O61−Fe3−O42	93.2(3)
O1−Fe1−N11	79.4(3)	O61−Fe2−N21	93.2(3)	O62−Fe3−O42	172.7(3)
O41−Fe1−N11	92.5(3)	N22−Fe2−N21	73.7(3)	O11−Fe3−O42	92.5(3)
N12−Fe1−N11	71.6(4)	N2−Fe2−N21	90.2(3)	O51−Fe3−O42	90.7(3)
O61−Fe1−Cl1	108.0(2)	O62−Fe2−N1	96.8(3)	O61−Fe3−O31	97.2(3)
O1−Fe1−Cl1	94.9(2)	O61−Fe2−N1	154.6(3)	O62−Fe3−O31	89.3(3)
O41−Fe1−Cl1	91.5(3)	N22−Fe2−N1	88.5(3)	O11−Fe3−O31	172.9(3)
N12−Fe1−Cl1	164.3(3)	N2−Fe2−N1	72.4(3)	O51−Fe3−O31	89.6(3)
N11−Fe1−Cl1	93.3(3)	N21−Fe2−N1	94.9(3)	O42−Fe3−O31	85.7(3)
O62−Fe4−O21	90.1(3)	O52−Fe4−N32	86.6(3)	O62−Fe4−Cl2	106.4(2)
O52−Fe4−O62	95.2(3)	O62−Fe4−N31	159.4(3)	O21−Fe4−Cl2	96.9(2)
O21−Fe4−O52	167.9(3)	O21−Fe4−N31	83.0(3)	O52−Fe4−Cl2	92.0(2)
O62−Fe4−N32	86.8(3)	O52−Fe4−N31	88.3(3)	N32−Fe4−Cl2	166.8(2)
O21−Fe4−N32	82.8(3)	N32−Fe4−N31	73.1(3)	N31−Fe4−Cl2	93.7(2)
Fe1−O61−Fe2	126.7(3)	Fe1−O61−Fe3	114.8(3)	Fe2−O61−Fe3	95.8(3)
Fe2−O62−Fe4	126.2(3)	Fe3−O62−Fe4	114.9(3)	Fe2−O62−Fe3	95.7(3)

Chart 2. Three Types of "Butterfly" Configurations Discussed in Table 4

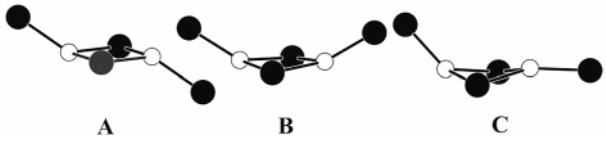

Scheme 2. Diagram of the $[Fe_4(\mu_3\text{-}O)_2]^{8+}$ Core Defining Its Metrical Parameters

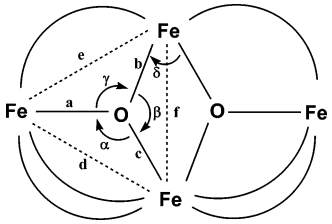

around the Fe^{III} ions. Two of the $(py)_2CNO^-$ ligands are coordinated to the "body" Fe2 through their pyridine and oximato N atoms, whereas they use their oximato O atom to bridge one of the "wingtip" ions, Fe1 and Fe4. In this way, Fe2 presents an O_2N_4 distorted octahedral coordination. The remaining two $(py)_2CNO^-$ ligands are coordinated through their pyridine and oximato N atoms to the "wingtip" ions Fe1 and Fe4, respectively, whereas their oximato O atom is bridging the "body" ion Fe3. The "body" Fe3 ion is also bridged to each of the "wingtip" ions Fe1 and Fe4 through a *syn,syn*-η^1:η^1:μ_2 acetato group. The octahedral coordination around each of the "wingtip" Fe^{III} ions in complexes **1a** and **1b** is completed by a Cl^- ion. In this manner, Fe3 presents an O-rich octahedral coordination environment, while Fe1 and Fe4 present an O_3N_2Cl octahedral coordination. The second pyridyl group of each $(py)_2CNO^-$ ligand remains uncoordinated.

The molecular structure of **2** is shown in Figure 2, and selected bond distances and angles are listed in Table 3. The structure is completely analogous to those of **1a** and **1b**, with the only difference being the terminal azide completing the octahedral coordination around each of the "wingtip" Fe^{III} ions instead of the Cl^- ion in the case of **1a** and **1b**. The structural characteristics of the $[Fe_4(\mu_3\text{-}O)_2]^{8+}$ "butterfly" core in **2** are summarized in Table 4 along with those of **1a** and **1b**.

Mössbauer Spectroscopy. Mössbauer spectra of **1a** and **2** were collected between 4.2 and 300 K. The spectra at 300 K are shown in Figure 3. The Mössbauer spectrum of **1a** at 300 K consists of a symmetric quadrupole-split doublet with parameters typical of high-spin ferric sites in octahedral environments. The large $\Gamma_{1/2}$ value and loss of symmetry upon cooling indicate that this is a composite doublet. The Mössbauer spectrum of **2** consists of an asymmetric composite quadrupole-split doublet with parameters similar to those of **1a**.

It is worth noting that the sole structural difference between **1a** and **2** lies in the replacement of the terminal chlorides in **1a** by terminal azides in **2**. This replacement brings about distinctive differences in the appearance of the Mössbauer spectra, which stresses the different donor atom effects produced by chlorides and azides. Inspection of the structures reveals three different Fe sites for each complex, with respect to their coordination spheres. **1a** contains sites with O_6 (Fe3), O_3ClN_2 (Fe1 and Fe4), and O_2N_4 (Fe2) chromophores,

Table 3. Selected Bond Distances (Å) and Angles (deg) in **2**·2CH_2Cl_2·2.5H_2O

		Distances			
Fe1−O61	1.882(5)	Fe2−O61	1.895(5)	Fe3−O61	1.986(5)
Fe1−O1	2.033(5)	Fe2−O62	1.897(5)	Fe3−O62	1.991(5)
Fe1−O41	2.038(6)	Fe2−N22	2.135(7)	Fe3−O31	1.999(5)
Fe1−N41	2.066(8)	Fe2−N2	2.154(7)	Fe3−O11	2.018(5)
Fe1−N12	2.159(7)	Fe2−N1	2.210(7)	Fe3−O42	2.027(6)
Fe1−N11	2.195(7)	Fe2−N21	2.222(7)	Fe3−O51	2.029(5)
Fe4−O62	1.882(5)	Fe4−O52	2.051(6)	Fe4−N32	2.165(6)
Fe4−O21	2.026(6)	Fe4−N51	2.078(8)	Fe4−N31	2.200(7)
Fe1···Fe2	3.366(2)	Fe1···Fe3	3.259(2)	Fe1···Fe4	5.967(2)
Fe2···Fe3	2.887(2)	Fe2···Fe4	3.377(2)	Fe3···Fe4	3.264(2)
		Angles			
O61−Fe1−O1	90.1(2)	O62−Fe2−O61	86.4(2)	O62−Fe3−O61	81.5(2)
O61−Fe1−O41	95.9(2)	O61−Fe2−N22	118.0(2)	O61−Fe3−O31	95.4(2)
O1−Fe1−O41	170.4(2)	O62−Fe2−N22	84.7(2)	O62−Fe3−O31	90.2(2)
O61−Fe1−N41	106.9(3)	O61−Fe2−N2	84.5(2)	O61−Fe3−O11	90.2(2)
O1−Fe1−N41	94.4(3)	O62−Fe2−N2	118.9(2)	O11−Fe3−O62	95.4(2)
O41−Fe1−N41	91.1(3)	N22−Fe2−N2	149.6(3)	O31−Fe3−O11	172.6(2)
O61−Fe1−N12	85.7(2)	O61−Fe2−N1	154.5(2)	O61−Fe3−O42	93.8(2)
O1−Fe1−N12	85.1(2)	O62−Fe2−N1	94.7(2)	O62−Fe3−O42	172.4(2)
O41−Fe1−N12	87.8(2)	N22−Fe2−N1	87.4(3)	O31−Fe3−O42	84.2(2)
N12−Fe1−N(41)	167.4(3)	N2−Fe2−N1	72.6(3)	O11−Fe3−O42	90.7(2)
O61−Fe1−N11	156.7(2)	O61−Fe2−N2	95.2(2)	O61−Fe3−O51	170.8(2)
O1−Fe1−N11	80.2(2)	O62−Fe2−N221	155.1(2)	O62−Fe3−O51	93.2(2)
O41−Fe1−N11	91.5(3)	N22−Fe2−N21	72.7(3)	O51−Fe3−O31	92.2(2)
N41−Fe1−N11	95.0(3)	N2−Fe2−N21	85.9(3)	O51−Fe3−O11	82.7(2)
N12−Fe1−N11	72.5(2)	N21−Fe2−N1	94.4(3)	O42−Fe3−O51	92.3(2)
O62−Fe4−O21	89.4(2)	O52−Fe4−N51	91.3(3)	O62−Fe4−N31	157.2(2)
O52−Fe4−O62	95.9(2)	O62−Fe4−N32	86.8(2)	O21−Fe4−N31	80.9(2)
O21−Fe4−O52	170.4(2)	O21−Fe4−N32	87.0(2)	O52−Fe4−N31	91.2(2)
O62−Fe4−N51	108.0(2)	O52−Fe4−N32	85.3(2)	N51−Fe4−N31	93.4(3)
O21−Fe4−N51	94.7(3)	N32−Fe4−N51	165.1(2)	N32−Fe4−N31	72.2(2)
Fe1−O61−Fe2	126.0(3)	Fe1−O61−Fe3	114.8(2)	Fe2−O61−Fe3	96.1(2)
Fe2−O62−Fe4	126.7(3)	Fe3−O62−Fe4	114.9(2)	Fe2−O62−Fe3	95.9(2)

Table 4. Comparison of Selected Structural Parameters (Å, deg) of Some Fe^{III} "Butterly" Complexes Possessing the $[Fe_4(\mu_3\text{-}O)_2]^{8+}$ Core[a]

complex	α	β	γ	δ	*a*	*b*	*c*	*d*	*e*	*f*	type[b]	ref
1a·2CH_2Cl_2·H_2O	115.15	97.25	125.65	82.75	1.886	1.906	1.980	3.2625	3.3735	2.916	**C**	this work
1b·4.5$MeNO_2$	114.8	95.75	126.45	84.15	1.880	1.912	1.9855	3.257	3.3845	2.890	**C**	this work
2·2CH_2Cl_2·2.5H_2O	114.75	96.0	126.3	83.95	1.882	1.896	1.989	3.262	3.372	2.887	**C**	this work
$[Fe_4O_2(BICOH)_2(BICO)_2(O_2CPh)_4]^{2+}$ [c]	119.0	95.7	136.8	84.3	1.884	1.980	1.940	3.290	3.590	2.900	**A**	25a
$[Fe_4O_2(O_2CCF_3)_8(H_2O)_6]$	133.9	96.5	129.5	82.9	1.842	1.961	1.936	3.476	3.436	2.915	**A**	25b
$[Fe_4O_2(O_2CPh)_7\{H_2B(pz)_2\}_2]^-$ [d]	125.15	93.5	133.6	85.4	1.822	1.955	1.895	3.326	3.488	2.829	**B**	26a
$[Fe_4O_2(O_2CMe)_7(bpy)_2]^+$	123.91	95.0	131.9	84.45	1.819	1.926	1.947	3.306	3.439	2.855	**B**	26b
$[Fe_4O_2Cl_2(O_2CMe)_6(bpy)_2]$	124.25	95.05	130.05	82.45	1.813	1.9345	1.992	3.314	3.454	2.896	**C**	27a
$[Fe_4O_2(N_3)_2(O_2CMe)_6(phen)_2]$	125.5	95.1	129.45	83.45	1.827	1.973	1.9355	3.344	3.346	2.884	**C**	27b

[a] See Scheme 2 to identify the bond lengths and angles. [b] See Chart 2. [c] BICOH = bis(*N*-methylimidazol-2-yl)carbinol. [d] $H_2B(pz)_2^-$ = dihydrobis(1-pyrazolyl)borate.

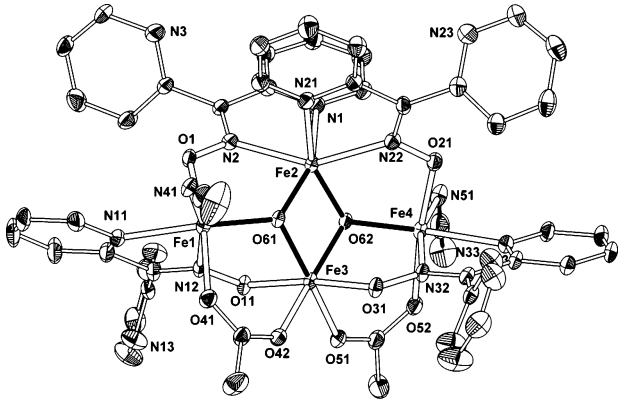

Figure 2. Partially labeled ORTEP plot of **2** with ellipsoids drawn at the 30% probability level. H atoms have been omitted for clarity. Black bonds describe the $[Fe_4(\mu_3\text{-}O)_2]^{8+}$ core.

whereas **2** contains sites with O_6 (Fe3), O_3N_3 (Fe1 and Fe4), and O_2N_4 (Fe2) chromophores. Given the relatively small dependence of Mössbauer parameters (δ and ΔE_Q) on the coordination environment (donor atoms and geometry) for high-spin ferric ions, it is clear that a rigorous assignment of the spectra would lack physical meaning in the present case because it would require the fitting of spectra with few distinctive features by considering three different sites.

We therefore proceed with a qualitative analysis of the spectra of **1a** and **2** at 300 K. The spectrum of **1a** is fitted with a single quadrupole-split doublet, whereas that of **2** is fitted with two doublets in order to account for the asymmetry and the shoulder of the negative velocity peak. The results are given indicatively and not for purposes of site assignment. Thus, fitting of the data of **1a** yields parameters $\delta = 0.36$ mm s^{-1}, $\Delta E_Q = 0.70$ mm s^{-1}, and $\Gamma_{1/2} = 0.29$ mm s^{-1}, and fitting of the data of **2** yields parameters $\delta_1 = 0.34$ mm s^{-1}, $\Delta E_{Q1} = 1.04$ mm s^{-1}, $\Gamma_{1/2(1)} = 0.15$ mm s^{-1}, and $A_1 = 26\%$ and $\delta_2 = 0.40$ mm s^{-1}, $\Delta E_{Q2} = 0.58$ mm s^{-1}, $\Gamma_{1/2(2)} = 0.17$ mm s^{-1}, and $A_2 = 74\%$.

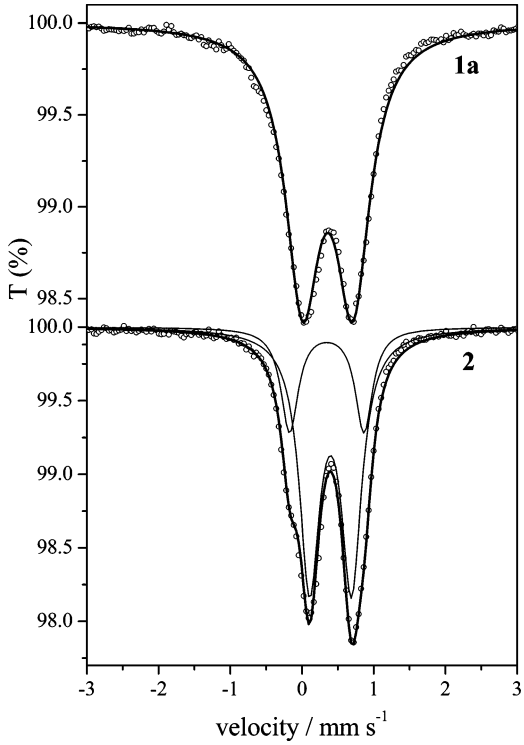

Figure 3. Mössbauer spectra of **1a** and **2** at 300 K. Indicative fits have been carried out as described in the text.

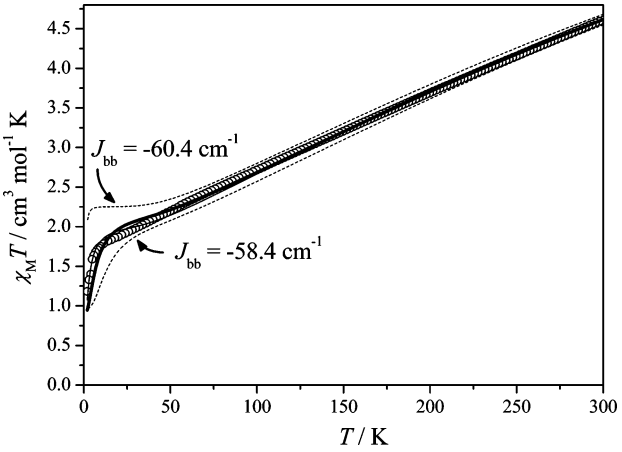

Figure 4. $\chi_M T$ vs T experimental data for complex **1a** and the best-fit theoretical curves based on the Hamiltonian of eq 4 and solutions **A** (thin line) and **B** (thick line). Calculations with J_{bb} values differing by ± 1 cm^{-1} from the best-fit value of solution **B** are shown as dashed lines.

Magnetic Susceptibility Measurements. The $\chi_M T$ product at 300 K is 4.61 cm^3 mol^{-1} K for **1a** (Figure 4), significantly lower than the theoretically expected value for four noninteracting $S = {}^5/_2$ ions (17.52 cm^3 mol^{-1} K), indicating dominant antiferromagnetic interactions. This is also indicated by the constant decrease of the $\chi_M T$ product upon cooling, down to a value of 1.18 cm^3 mol^{-1} K at 2 K. The χ_M vs T curve shows a continuous increase upon cooling.

The metal core of **1a** adopts a "butterfly" geometry (see the Description of the Structures section), with Fe1 and Fe4 occupying the "wingtip" positions and Fe2 and Fe3 the "body" ones. A rigorous interpretation of the magnetic susceptibility data would require the consideration of two exchange coupling constants for the wingtip−body interactions, one for the Fe(O_{oxo})(N−O_{oxime})Fe bridged pairs Fe1/Fe2 and Fe2/Fe4 and one for the Fe(O_{oxo})(N−O_{oxime})($MeCO_2$)-Fe bridged pairs Fe1/Fe3 and Fe3/Fe4, and a third for the body−body interaction. However, this proved to overparametrize the problem, so only two interactions were considered, one between wingtip−body atoms (J_{wb}) and one between body−body atoms (J_{bb}). The corresponding spin Hamiltonian is thus written as

$$\hat{H} = -2[J_{wb}(\hat{\mathbf{S}}_1\hat{\mathbf{S}}_2 + \hat{\mathbf{S}}_1\hat{\mathbf{S}}_3 + \hat{\mathbf{S}}_3\hat{\mathbf{S}}_4 + \hat{\mathbf{S}}_2\hat{\mathbf{S}}_4) + J_{bb}(\hat{\mathbf{S}}_2\hat{\mathbf{S}}_3)] \quad (4)$$

When the g factor was fixed at 2.0, as would be expected for an isotropic high-spin Fe^{III} ion, no satisfactory solution could be obtained with this model. Release of this parameter led to a satisfactory solution with best-fit parameters $J_{wb} = -34.3$ cm^{-1}, $J_{bb} = -51.1$ cm^{-1}, and $g = 1.91$ with $R = 3.6 \times 10^{-4}$ (solution **A**). These parameters yield an $S = 1$ ground state, with an $S = 2$ excited state at 3.5 cm^{-1} and an $S = 0$ excited state at 98.7 cm^{-1}. This result is rather surprising because Fe^{III}_4 butterfly complexes display antiferromagnetic interactions and possess $S = 0$ ground states. Because of small discrepancies over the low-temperature range, fits were carried out over the 300−34 K range in order to verify the derived J values. This induced a remarkable improvement to the fit, yielding a solution with best-fit parameters $J_{wb} = -40.2$ cm^{-1}, $J_{bb} = -59.4$ cm^{-1}, and $g = 2.0$ (fixed) with $R = 8.0 \times 10^{-5}$ (solution **B**). This solution entails again an $S = 1$ ground state, with an $S = 2$ excited state at 7.9 cm^{-1} and an $S = 0$ excited state at 110 cm^{-1}, with the g factor this time at 2.0. The derived J_{wb} values in each case fall within the range previously determined for other Fe^{III} "butterfly" complexes (Table 5). What can be observed for each solution is that, despite some variations of the J and g parameters, the J_{bb}/J_{wb} ratio remains close to 1.48. As will be seen later, the value of this ratio influences critically the energy mapping of the spin manifolds.

To obtain further verification of these findings, a magnetization isotherm was recorded for **1a** at 2 K (Figure 5). The M vs H curve nearly saturates at a moment of $\sim 1.98 N_A \mu_B$ (5.4 T) as expected for an $S = 1$ spin. Calculations with the parameters of solutions **A** and **B**, as well as an $S = 1$ Brillouin curve ($g = 2$), are shown in Figure 5. From these, we deduce that solution **B** is in a better agreement with the M vs H experimental data, despite some discrepancies at low temperatures in the $\chi_M T$ vs T plot. The $S = 1$ Brillouin curve

Table 5. Comparison of Exchange Coupling Constants of Some Fe^{III}_4 Complexes with Similar Spin Topologies

complex	J_{wb} (J_{bb}) (cm^{-1})[a]	ref
1a	**−40.2 (−59.4)**	this work
$[Fe_4O_2(O_2CCMe_3)_8(NC_5H_4Me)_2]$	−37.2 (*0*)	28
$[Fe_4O_2(O_2CPh)_8(phen)_2]$	−32.9 (−7.8)	29
$[Fe_4O_2Cl_2(O_2CMe)_6(bpy)_2]$	NR (−10.9)	27a
$[Fe_4O_2(N_3)_2(O_2CMe)_6(phen)_2]$	−35 (−5.5)	27b
$[Fe_4O_2(O_2CPh)_7(phen)_2](ClO_4)$	−38.8 (−1.2)	29
$[Fe_4O_2(O_2CMe)_7(bpy)_2](ClO_4)$	−45.5 (−8.9)	26b
$[Fe_4O_2L_2(salox)_2\{O_2C(OH)Ph_2\}_3](ClO_4)$[b]	−41.4 (*0*)	30

[a] $H = -2\sum J_i J_j$ and $g = 2.0$. Values in italics were fixed. NR = not reported. [b] L = 1,4,7-trimethyl-1,4,7-triazacyclononane; $salox^{2-}$ = dianion of salicylaldehyde oxime.

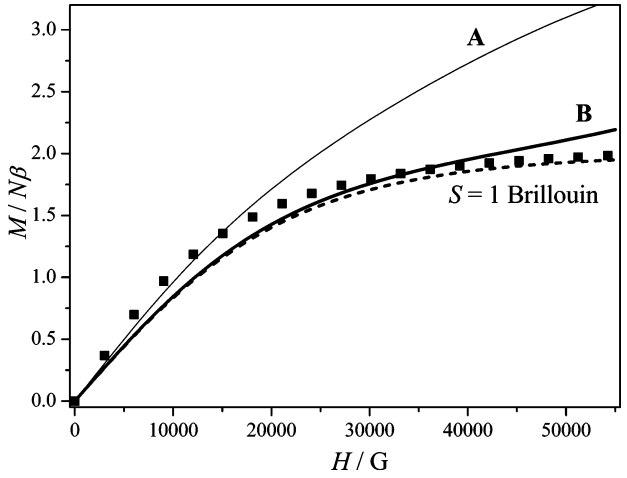

Figure 5. Magnetization M vs applied magnetic field H data (■) at 2 K for complex **1a**. The calculated curves are based on the parameters of solutions **A** (thin line) and **B** (thick line) and on an $S = 1$ Brillouin curve (dashed line).

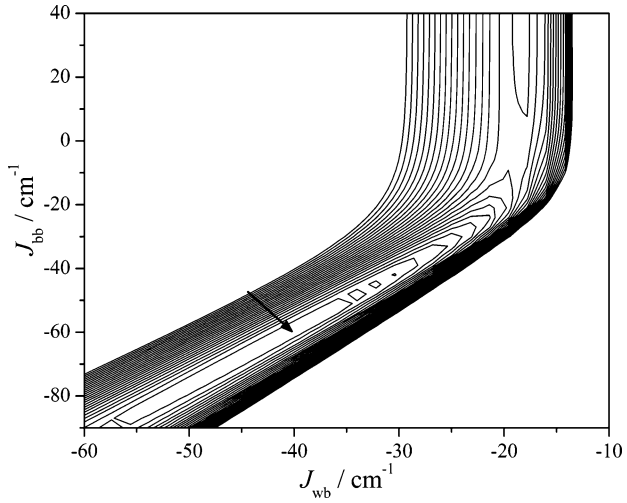

Figure 6. Error contour plot for different J_{wb} and J_{bb} values. Calculations were carried out for $g = 2.0$. The arrow indicates the position of the best-fit solution.

at 2 K is also very adequate in reproducing the magnetization data at low temperatures, thus providing further evidence for an $S = 1$ ground state in **1a**. Some disagreement between experimental and calculated values might be attributed to non-Heisenberg interactions and single-ion anisotropies that have not been included in the present model. Despite that, however, it remains clear that the ground state of **1a** is characterized by a total spin of $S = 1$.

To verify the uniqueness of this solution, an exploration of the (J_{wb}, J_{bb}) parameter space was carried out by drawing an error contour plot of J_{wb} vs J_{bb} (Figure 6). For similar complexes, the minima resemble long fosses, corresponding to well-determined J_{wb} values and indeterminate J_{bb} values.[26b]

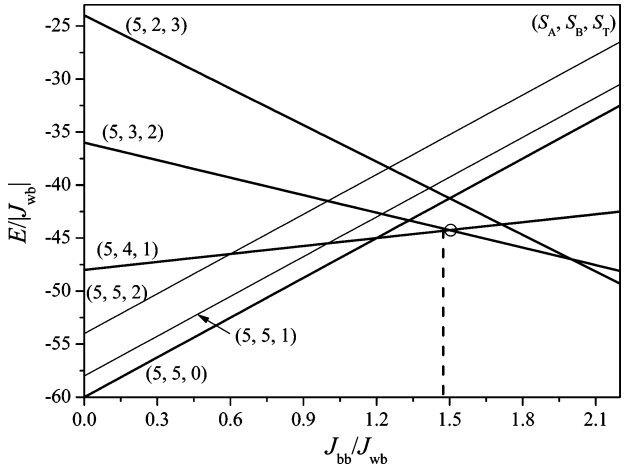

Figure 7. Selected energy-level diagrams showing the ground-state variation with respect to the J_{bb}/J_{wb} ratio. The dashed line marks the position of the J_{bb}/J_{wb} ratio for **1a**, and the circle indicates the transition point from an $S_T = 1$ to 2 ground state. Numbers in parentheses correspond to (S_A, S_B, S_T), where $S_A = S_1 + S_4$, $S_B = S_2 + S_3$, and $S_T = S_A + S_B$.

The error level plot for **1a**, however, confirmed our solution as a well-defined minimum. To illustrate this, simulations with different J_{bb} values were carried out (Figure 4) and compared to the experimental data and best-fit curve. In the simulations, all parameters were fixed to their best-fit values, and J_{bb} was set to ± 1 cm^{-1} with respect to its best-fit value (i.e., $\sim\pm 1.5\%$). The resulting curves were significantly different from the best-fit one, indicating that the value of the parameter is well determined and significantly influences the global behavior.

To assess the sensitivity of our fits to the absolute values of J_{wb} and J_{bb}, $\chi_M T$ vs T calculations were carried out for J_{wb} values fixed at ± 1 cm^{-1} from its best-fit value (-40.2 cm^{-1}), while fixing the J_{bb} value so as to keep the J_{bb}/J_{wb} ratio constant to 1.48 [(J_{wb}, J_{bb}) = (-41.2 cm^{-1}, 60.9 cm^{-1}) and (-39.2 cm^{-1}, 57.9 cm^{-1})] derived from the best-fit solution. The calculated curves (Figure S2 in the Supporting Information) are practically superimposable at low temperatures, where the ground-state population is predominant, but they diverge at higher temperatures, where excited spin states are populated, with populations depending on their absolute energies and therefore on the absolute J values. The agreement factors R for these two parameter sets are 2.2×10^{-4} and 2.1×10^{-4}, respectively. Thus, for only a 1-cm^{-1} difference in J_{wb} ($\sim\pm 2\%$), we observe an increase of R by a factor of ~ 3, which means that the curve is sensitive to the absolute values of J_{wb} and J_{bb} as well.

To rationalize the $S = 1$ ground state of **1a**, as well as the well-determined value of the J_{bb} parameter, we show a

(25) Among many others, see, for example: (a) Gorum, S. M.; Lippard, S. J. *Inorg. Chem.* **1988**, *27*, 149. (b) Ponomarev, V. I.; Atovmyan, L. O.; Bobkova, S. A.; Turte, K. I. *Dokl. Akad. Nauk SSSR* **1984**, *274*, 368.

(26) Among many others, see, for example: (a) Armstrong, W. H.; Roth, M. E.; Lippard, S. J. *J. Am. Chem. Soc.* **1987**, *109*, 6318. (b) McCusker, J. K.; Vincent, J. B.; Schmitt, E. A.; Mino, M. L.; Shin, J.; Coggin, D. A. K.; Hagen, P. M.; Huffman, J. C.; Christou, G.; Hendrickson, D. N. *J. Am. Chem. Soc.* **1991**, *113*, 3012.

(27) (a) Wemple, M. W.; Coggin, D. A. K.; Vincent, J. B.; McCusker, J. K.; Streib, W. E.; Huffman, J. C.; Hendrickson, D. N.; Christou, G. *J. Chem. Soc., Dalton Trans.* **1998**, 719. (b) Boudalis, A. K.; Tangoulis, V.; Raptopoulou, C. P.; Terzis, A.; Tuchagues, J.-P.; Perlepes, S. P. *Inorg. Chim. Acta* **2004**, *357*, 1345.

(28) Overgaard, J.; Hibbs, D. E.; Rentschler, E.; Timco, G. A.; Larsen, F. K. *Inorg. Chem.* **2003**, *42*, 7593.

(29) Boudalis, A. K.; Lalioti, N.; Spyroulias, G. A.; Raptopoulou, C. P.; Terzis, A.; Bousseksou, A.; Tangoulis, V.; Tuchagues, J.-P.; Perlepes, S. P. *Inorg. Chem.* **2002**, *41*, 6474.

(30) Chaudhuri, P.; Rentschler, E.; Birkelbach, F.; Krebs, C.; Bill, E.; Weyhermüller, T.; Flörke, U. *Eur. J. Inorg. Chem.* **2003**, 541.

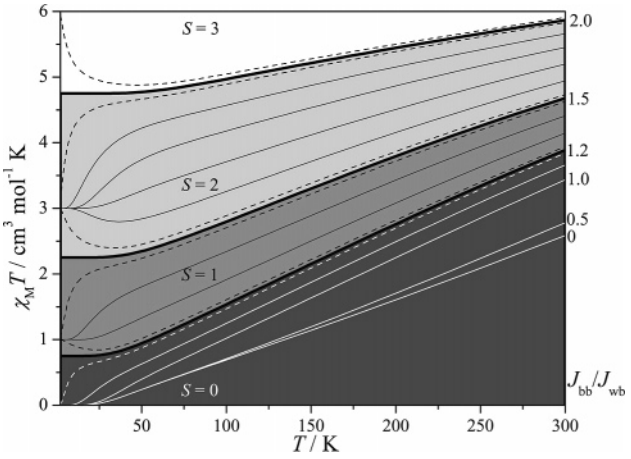

Figure 8. Calculated $\chi_M T$ vs T curves for a spin system similar to that of **1a** ($J_{wb} = -40$ cm^{-1} and $g = 2.0$) and for various J_{bb}/J_{wb} values (indicative values shown on the right). Thick black lines represent simulations for the special cases where J_{bb}/J_{wb} is 1.2, 1.5, and 2.0. Dashed lines represent simulations for the cases where J_{bb}/J_{wb} is 0.02 below or above these values. Intermediate continuous lines between 1.0 and 2.0 are drawn for 0.1 increments of the J_{bb}/J_{wb} ratio. For clarity, different shades distinguish the curves corresponding to different ground states.

correlation diagram of selected low-lying spin-state energies as a function of the J_{bb}/J_{wb} ratio (Figure 7). As can be seen, for $J_{bb}/J_{wb} < 1.2$, the ground state is $S_T = 0$. For $1.2 < J_{bb}/J_{wb} < 1.5$, the ground state is $S_T = 1$, and for $1.5 < J_{bb}/J_{wb} < 2.0$, the ground state is $S_T = 2$. In the special cases of $J_{bb}/J_{wb} = 1.2$, 1.5, or 2.0, a degeneracy appears in the ground state between states with total spins $S_T = 0$ and 1, 1 and 2, and 2 and 3, respectively. Therefore, for ca. $0.5 < J_{bb}/J_{wb} < 2.0$, variations of J_{bb}/J_{wb} will significantly influence the total energy-level diagram of the system and its magnetic susceptibility, leading to a well-determined J_{bb}. In the case of **1a** in particular, the value of this ratio is ~1.48, very close to the transition point at 1.5 between the $S_T = 1$ and 2 states. Around this region, very small variations of J_{bb} will lead to severe variations of the energy spectrum of the complex, causing the J_{bb} value to be even better determined. Following this reasoning, we could therefore attribute the previously reported indeterminacy of J_{bb} to the J_{bb}/J_{wb} dependence of the low-lying magnetic states; for J_{bb}/J_{wb} of less than ca. 0.5, the lowest-lying excited magnetic states (5, 5, 1) and (5, 5, 2) are separated by $2J_{wb}$ and $6J_{wb}$ from (5, 5, 0), respectively. These separations are constant and do not depend on J_{bb}/J_{wb}. Therefore, J_{bb}/J_{wb} variations in that region would not particularly influence the energies of the low-lying magnetic states of the energy spectrum, and consequently the magnetic susceptibility would be rather insensitive to J_{bb}. This means that the indeterminacy of J_{bb} is not physical but rather stemming from the use of susceptometry data to derive exchange couplings. These have been analyzed in detail previously.[26b]

To the best of our knowledge, **1a** is the first butterfly-like high-spin ferric complex with an $S = 1$ ground state. In comparison with other similar complexes that exhibit an $S = 0$ ground state, the unique feature of **1a** is the magnitude of J_{bb}, whereas J_{wb} varies between ca. -33 and -46 cm^{-1} (Table 5). It would be helpful therefore to examine the temperature dependence of the magnetic susceptibility data for various values of the J_{bb}/J_{wb} ratio. We have chosen $J_{wb} = -40$ cm^{-1} as a reasonable average value (Table 5), $g = 2.0$, and varied J_{bb}. Theoretical simulations of the temperature variation of $\chi_M T$ for various values of J_{bb}/J_{wb} between 0 and 2 are shown in Figure 8. As can be seen for $0 < J_{bb}/J_{wb} < 0.5$, the variation of the $\chi_M T$ vs T curve is very small. Above $J_{bb}/J_{wb} \sim 0.5$, the variations are more important and clearly discernible. Near the transition points at 1.2, 1.5, and 2.0, small variations of J_{bb}/J_{wb} by only 0.02 lead to dramatic changes, particularly in the low-temperature region.

Conclusions

The present work extends the body of results that emphasize the ability of the anionic ligand $(py)_2CNO^-$ to form interesting clusters in 3d metal chemistry. We have conducted a thorough study of the parameter space of the $Fe^{III}/MeCO_2^-/(py)_2CNOH$ reaction system in the presence of Cl^- or N_3^-. From this study, it was established that the Fe^{III}_4 "butterfly" core is stable, irrespective of the type of anions present in the reaction mixture (Cl^- or N_3^-). Therefore, we were able to obtain the same products through different synthetic routes and to achieve transformations between them through ligand exchange. In addition, the terminal chloro and azido ligands in **1** and **2** could have future synthetic utility as sites for the incorporation of other monodentate ligands by metathesis or as a means to obtain higher nuclearity complexes using anionic bis(monodentate) bridging ligands. Although the variety of Fe sites present in the complexes is too great for a quantitative interpretation of the Mössbauer spectra, it was concluded that replacement of chlorides with azides in the complexes provokes significant differences in their appearance. The magnetic study of **1a** revealed that this complex possesses an $S = 1$ ground state because of the particular value of the J_{bb}/J_{wb} ratio. In addition, it was concluded that the indeterminacy of the J_{bb} parameter in "butterfly" complexes can be lifted when the J_{bb}/J_{wb} ratio acquires values for which a multitude of low-lying spin states with different S_T are close in energy or, more so, when the J_{bb}/J_{wb} ratio acquires values near transition points of the ground state's total spin, S_T, around which the magnetic behavior is expected to be a more sensitive function of J_{bb}/J_{wb}.

Acknowledgment. We thank Dr. Juan Modesto Clemente-Juan for helpful discussions. A.K.B. thanks the Greek State Scholarship Foundation (IKY) for support through a postdoctoral grant. Th.C.S. thanks the European Social Fund, Operational Program for Educational and Vocational Training II (EPEAEK II), and particularly the Program PYTHAGORAS (Grant b.365.037) for funding this work.

Supporting Information Available: X-ray crystallographic files, in CIF format, for **1a**, **1b**, and **2**, Table S1 with selected bond distances and angles for complex **1a**, and χ_M vs T plots and $\chi_M T$ vs T simulations for **1a** (Figures S1 and S2, respectively). This material is available free of charge via the Internet at http://pubs.acs.org.

IC0604821